processes

MDPI

Article

Study of Activation Energy on the Movement of Gyrotactic Microorganism in a Magnetized Nanofluids Past a Porous Plate

Muhammad Mubashir Bhatti [1], Anwar Shahid [2], Tehseen Abbas [3], Sultan Z Alamri [4] and Rahmat Ellahi [5,6,7,*]

1 College of Mathematics and Systems Science, Shandong University of Science & Technology, Qingdao 266590, China; mmbhatti@sdust.edu.cn
2 College of Astronautics, Nanjing University of Aeronautics & Astronautics, Nanjing 210016, China; anwar@nuaa.edu.cn
3 Department of Mathematics, University of Education Lahore, Faisalabad Campus, Faisalabad 38000, Pakistan; tehseen.abbas@ue.edu.pk
4 Faculty of Science, Taibah University Al-Madinah Al-Munawarah, Madinah 41411, Saudi Arabia; szamri@taibahu.edu.sa
5 Department of Mathematics and Statistics, International Islamic University, Islamabad 44000, Pakistan
6 Fulbright Fellow Department of Mechanical Engineering, University of California Riverside, Riverside, CA 92521, USA
7 Center for Modeling & Computer Simulation, Research Institute, King Fahd University of Petroleum and Minerals, Dhahran-31261, Saudi Arabia
* Correspondence: rellahi@alumni.ucr.edu

Received: 16 February 2020; Accepted: 5 March 2020; Published: 11 March 2020

Abstract: The present study deals with the swimming of gyrotactic microorganisms in a nanofluid past a stretched surface. The combined effects of magnetohydrodynamics and porosity are taken into account. The mathematical modeling is based on momentum, energy, nanoparticle concentration, and microorganisms' equation. A new computational technique, namely successive local linearization method (SLLM), is used to solve nonlinear coupled differential equations. The SLLM algorithm is smooth to establish and employ because this method is based on a simple univariate linearization of nonlinear functions. The numerical efficiency of SLLM is much powerful as it develops a series of equations which can be subsequently solved by reutilizing the data from the solution of one equation in the next one. The convergence was improved through relaxation parameters in the study. The accuracy of SLLM was assured through known methods and convergence analysis. A comparison of the proposed method with the existing literature has also been made and found an excellent agreement. It is worth mentioning that the successive local linearization method was found to be very stable and flexible for resolving the issues of nonlinear magnetic materials processing transport phenomena.

Keywords: electro-conductive polymer processing; porous media; bio-convection; gyrotactic microorganisms

1. Introduction

Recent betterments in nanotechnology arose through the investigation of the physical characteristics of matter at the nanoscale level. Multiple industrial utilizations of nanofluids established their growing use in heat transfer. The use of nanofluids has been promoted in assorted imperative subfields due to their thermal transport and captivating uses. Like their peculiarly

higher thermal conductivity, nanofluids have improved the stability that averts rapid establishing and choking adjacent to heat transfers across the boundaries of the materials. Exploring the stimulants in nanofluid, branches through the heat transfer enlargement into mechanisms comprising space-cooling, hybrid-powered engines, nuclear engineering, micro-manufacturing, microchips in computer processors, air-conditioners/refrigerators, fuel cells, diesel engine oil, and other higher energy equipment. Classical theory of the single-phase fluids is helpful for the nanofluids by observing the thermo-physical features of nanofluids, base fluids and their constituents. It is noteworthy that the thermal conductivity of the nanofluids is enhanced through volume fraction, particle size, temperature, and thermal conductivity. Buongiorno [1] promoted a nanofluid model to elaborate the propagation of thermal energy. Tiwari and Das [2] developed a simpler model through which thermos-physical characteristics were investigated as function of nanoparticle volume fraction. Kuznetsov and Nield [3] used a Buongiorno model to interpret the conduction of thermophoretic diffusion and Brownian motion on nanofluid flow neighboring a heating vertical surface through a pervious media and noted that both thermophoresis and Brownian-motion bring a decrement in heat transfer rate through the plate. As the standard of ultimate production relies on the heat transfer rate, as acknowledged, the nanofluids with a higher rate of thermal conductivity enhance the rate of heat transfer [4,5]. For this purpose, distinct techniques are adopted to raise the thermal conductivity of the fluids by providing the suspension of nano/micro- or large-sized particles into liquids. An inventive approach to enhance the heat transfer rate is performed by utilizing nano-scale particles into the base-fluid by Choi et al. [6]. They recorded that, by adding a tiny extent (<1%) of nanoparticles to regular heat transfer fluids, the thermal conductivity for fluids up to almost 4-times and higher was enhanced. Ellahi et al. [7] discussed the two-phase Newtonian nanofluid flow hybrid with hafnium particles under the effects of slip. Majeed et al. [8] scrutinized the stretched stretching sheet under the combine effects of suction, heat transfer and ferromagnetic viscoelastic fluid flow. Noghrehabadadi et al. [9] explored the flow and heat transfer of nanofluids past a stretched subsurface, supposing of thermal convectively boundary conditions and partial slip. Nilson and Griffiths [10] discussed the electro-osmotic flow with atomistic physics and presented a detailed analysis using density functional theory. Lee et al. [11] presented a comparative study on molecular dynamics via classical density function through a double layer nano-channels with the help of the poisson–boltzmann theory. Some important analyses on the nanofluid flow through various configurations are available in the references [12–16].

The magnetized stagnation flow past a stretched surface has numerous productive usages, such as glass industries, a tragedy core reducing system, and decontamination of crude oil. Theoretically, the boundary layer flow and the flow causes from a stretching plate are fairly imperative. Hiemenz [17] first introduced the stagnation point flow in a two-dimensional channel. Chiam [18] scrutinized the stretching and strain rate of the stagnation point flow of the sheet and observed that boundary layers do not occur close to the sheet. Asma et al. [19] numerically inspected the magnetized nanofluid motion over a rotating disk with activation energy and binary chemical formulation. It is important to mention here that Makinde and Animasaun [20] investigated an admirable work related to magnetized nanofluid flow alongside quartic autocatalysis chemical reaction and bio-convection, and recorded that, for a fixed numeric of magnetic parameters, the local skin friction further develops at a larger thickened parametric value, whereas the rate of local heat transfer decreases at high-temperature parametric values past an uppermost subsurface of a paraboloid of uprising. Scrutinizing the definitive utilities for nanofluid and MHD, few recent investigations can be found [21–38].

Activation energy is the minimum supply of energy needed to accomplish a chemical reaction. Very few researchers have studied the activation energy along with chemical reaction to date. Sajid et al. [39] scrutinized activation energy with nonlinear thermal radiation on the Maxwell Darcy-Forchheimer nanofluid flow. The impact of activation energy with radiative stagnation point flow on cross nanofluid was determined by Ijaz et al. [40]. Khan et al. [41] presented a theoretical report on tangent hyperbolic nanofluid alongside a fused electrical magnetic field, with Wu's slip and activation energy aspects. A few other analyses of activation energy are given in [42–44].

Bio-convection has many utilizations, similar to model oil, microbial enhanced oil recovery (EOR) and gas-bearing sedimentary basins. Due to this, some researchers have analyzed the mechanisms of several bio-convection obstacles providing suspended solid particles. The microbial EOR is a new technological process for gas and oil production and enhancing oil restoration. This mechanism involves the insertion of the preferred microorganisms into the containers and the residual oil left in the reservoir is reduced through in situ amplification when secondary restoration is exhausted. The self-impelled motile microorganisms enhanced the density of the base fluid in a peculiar way to produce a bio-convection kind of stream. Based on the cause of propulsion, the motile microorganisms perhaps categorized into various kinds of microorganisms, including oxytactic or chemotaxis, gyrotactic microorganisms, and negate gravitaxis. Unlike the motile microorganisms, the nanoparticles are not self-propelled, and their movement is through the thermophoresis and Brownian motion, impacting the inward nanofluid. Kuznetsov and Avramenko [45] analyzed bio-convection into a suspension of gyrotactic microorganisms through a layer of finite depth. This conception was extended by Kuznetsov and Geng [46] to numerous bio-convection problems. Lee et al. [47] experimentally interpreted the effects of convention in heated plate-fin. Khan and Makinde [48] examined nanofluid bio-convection caused by gyrotactic-microorganisms and they perceived that the microorganisms amplify the base-fluid density through floating/swimming in a specific manner. Recently, Raees et al. [49] interpreted that bio-convection into nanofluids has made enormous contributions to the Colibri micro-volumes spectrometer and benefitted the stability of nanofluids. Some other studies relating to gyrotactic microorganisms can be viewed here [50,51].

The intention of the current analysis is to examine the impact of an activation energy on magnetized fluid comprising of nanoparticles and motile gyrotactic microorganisms, flowing through a stretchable permeable sheet, by employing a successive local linearization method [52,53] not yet available in the existing literature. The current study scrutinizes the transporting phenomena into a nanofluid consisting of self-impelled motile gyrotactic microorganisms by providing a non-uniform magnetic field and convective cooling processes. The thermophoresis, Brownian-motion, and convectively cooling phenomena are also examined. Numerical results are displayed, and comparability with previous investigations is also provided for the validity of the current results.

2. Modeling

Let a bi-dimensional incompressible viscous, steady, and magnetized nanofluid flow comprising gyrotactic microorganisms through a stretched porous sheet filling porous space be assumed, as shown in Figure 1.

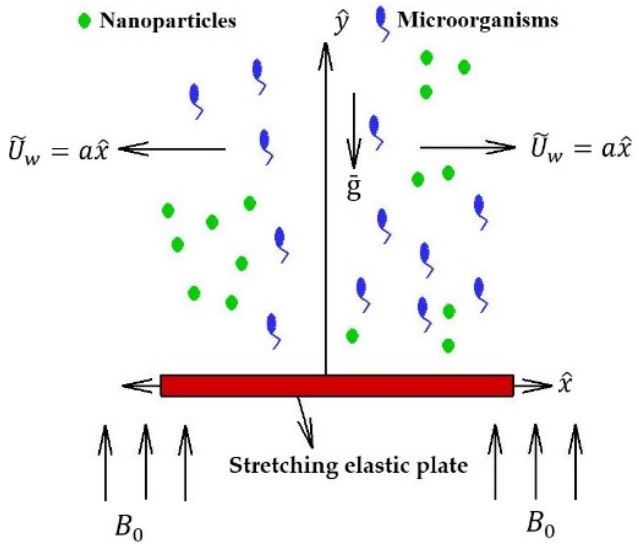

Figure 1. Geometry for the flow problem.

The leading equations for continuity, momentum, thermal energy, nanoparticle concentration, and microorganisms [54] are

$$\frac{\partial \widetilde{v}}{\partial \hat{y}} + \frac{\partial \widetilde{u}}{\partial \hat{x}} = 0, \tag{1}$$

$$\begin{aligned} \frac{\partial \widetilde{u}}{\partial \hat{x}}\widetilde{u} + \frac{\partial \widetilde{u}}{\partial \hat{y}}\widetilde{v} = -\frac{\partial \widetilde{p}}{\partial \hat{x}} + \nu_f\left(\frac{\partial^2 \widetilde{u}}{\partial \hat{x}^2} + \frac{\partial^2 \widetilde{u}}{\partial \hat{y}^2}\right) + \overline{g}\beta\left(1 - \widetilde{C}_\infty\right)\left(\widetilde{T} - \widetilde{T}_\infty\right) \\ -\overline{g}\left(\rho_p - \rho_f\right)\left(\widetilde{C} - \widetilde{C}_\infty\right) - \overline{g}\gamma'\left(\rho_m - \rho_f\right)\left(\widetilde{N} - \widetilde{N}_\infty\right) - \sigma B_0^2\widetilde{u} - \frac{\nu_f}{k}\widetilde{u} - \frac{C_F\rho_f}{\sqrt{k}}\widetilde{u}^2, \end{aligned} \tag{2}$$

$$\frac{\partial \widetilde{p}}{\partial \hat{y}} = 0, \tag{3}$$

$$\widetilde{u}\frac{\partial \widetilde{T}}{\partial \hat{x}} + \widetilde{v}\frac{\partial \widetilde{T}}{\partial \hat{y}} = \overline{\alpha}\left[\frac{\partial^2 \widetilde{T}}{\partial \hat{x}^2} + \frac{\partial^2 \widetilde{T}}{\partial \hat{y}^2}\right] + \widetilde{\tau}\left[D_B\frac{\partial \widetilde{C}}{\partial \hat{y}}\frac{\partial \widetilde{T}}{\partial \hat{y}} + \frac{D_T}{T_\infty}\left\{\left(\frac{\partial \widetilde{T}}{\partial \hat{x}}\right)^2 + \left(\frac{\partial \widetilde{T}}{\partial \hat{y}}\right)^2\right\}\right] + \frac{\mu_f\overline{\alpha}}{\overline{k}}\left(\frac{\partial \widetilde{u}}{\partial \hat{y}}\right)^2 + \frac{\sigma\overline{\alpha}{B_0}^2}{\overline{k}}\widetilde{u}^2, \tag{4}$$

$$\widetilde{u}\frac{\partial \widetilde{C}}{\partial \hat{x}} + \widetilde{v}\frac{\partial \widetilde{C}}{\partial \hat{y}} = D_B\left[\frac{\partial^2 \widetilde{C}}{\partial \hat{x}^2} + \frac{\partial^2 \widetilde{C}}{\partial \hat{y}^2}\right] + \frac{D_T}{T_\infty}\left[\frac{\partial^2 \widetilde{T}}{\partial \hat{x}^2} + \frac{\partial^2 \widetilde{T}}{\partial \hat{y}^2}\right] - {k_r}^2\left(\widetilde{C} - \widetilde{C}_\infty\right)\left(\frac{\widetilde{T}}{T_\infty}\right)^m e^{\left(\frac{-E_a}{k_0\widetilde{T}}\right)}, \tag{5}$$

$$\widetilde{u}\frac{\partial \widetilde{N}}{\partial \hat{x}} + \widetilde{v}\frac{\partial \widetilde{N}}{\partial \hat{y}} + \frac{bW_C}{\left(\widetilde{C} - \widetilde{C}_\infty\right)}\left[\frac{\partial}{\partial \hat{y}}\left(\widetilde{N}\frac{\partial \widetilde{C}}{\partial \hat{y}}\right) + \frac{\partial}{\partial \hat{x}}\left(\widetilde{N}\frac{\partial \widetilde{C}}{\partial \hat{x}}\right)\right] = D_M\left(\frac{\partial^2 \widetilde{N}}{\partial \hat{x}^2} + \frac{\partial^2 \widetilde{N}}{\partial \hat{y}^2} + 2\frac{\partial^2 \widetilde{N}}{\partial \hat{x}\partial \hat{y}}\right), \tag{6}$$

Their respective boundary conditions can be read as

$$\widetilde{u} = a\hat{x}, \widetilde{v} = 0, \widetilde{T} = \widetilde{T}_w, \widetilde{C} = \widetilde{C}_w, \widetilde{N} = \widetilde{N}_w \text{at} \hat{y} = 0, \tag{7}$$

$$\widetilde{u} \to 0, \widetilde{N} \to \widetilde{N}_\infty, \widetilde{v} \to 0, \widetilde{T} \to \widetilde{T}_\infty, \widetilde{C} \to \widetilde{C}_\infty, \text{as} \hat{y} \to \infty. \tag{8}$$

In Equations (1)–(8), $\widetilde{u}$ and $\widetilde{v}$ are the velocity components, $\left(\frac{\widetilde{T}}{T_\infty}\right)^m e^{\left(\frac{-E_a}{k_0\widetilde{T}}\right)}$ is an Arrhenius function, m is the dimensionless exponent, $\widetilde{T}$ is the temperature, $\widetilde{C}$ is the concentration for nanoparticle, $\widetilde{N}$ is the density for motile microorganism, $\widetilde{p}$ the pressure, ρ_f, ρ_m, ρ_p are the densities of nanofluid, microorganisms, D_T is thermophoresis-diffusion coefficient, D_M is diffusivity of microorganisms, D_B is Brownian-diffusion coefficient, $\overline{k}$ is the thermal conductivity of nanofluid, σ is the electrical conductivity of nanofluid, γ is the average volume for a microorganisms, $\overline{\alpha} = \overline{k}/\left(\rho c_p\right)$ is the thermal diffusivity, k_r is chemical reaction rate, E_a activation energy, C_F is the Forchheimer coefficient, k_0 is the Boltzman constant, bW_C are constants, $\widetilde{\tau} = (\rho C)_p/(\rho C)_f$ is the proportion of the effected nanoparticle heat capacitance of the base-fluid, strength of magnetic field is $B(x) = B_0(\hat{x})$, velocity of stretched sheet is $\widetilde{U}_w = a\hat{x}$, positive constant is a, concentration is $\widetilde{C}_w$, temperature of the wall is $\widetilde{T}_w$, motile microorganisms' densities are $\widetilde{N}_\infty$ and $\widetilde{N}_w$, ambient concentration is $\widetilde{C}_\infty$ and ambient temperature is $\widetilde{T}_\infty$.

The similarity transformation variables are defined as follows

$$\left.\begin{aligned} \widetilde{u} = a\hat{x}g'(\eta), \ \widetilde{v} = -\sqrt{a\nu}g(\eta), \eta = \sqrt{\tfrac{a}{\nu}}\,\hat{y}, \\ \theta(\eta) = \tfrac{\widetilde{T} - \widetilde{T}_\infty}{\widetilde{T}_w - \widetilde{T}_\infty}, \phi(\eta) = \tfrac{\widetilde{C} - \widetilde{C}_\infty}{\widetilde{C}_w - \widetilde{C}_\infty}, \Phi(\eta) = \tfrac{\widetilde{N} - \widetilde{N}_\infty}{\widetilde{N}_w - \widetilde{N}_\infty}. \end{aligned}\right\} \tag{9}$$

Using Equation (9) in Equations (1)–(8), we have

$$g''' + gg'' - g'^2 - Mg' - \beta_D g' - F_r g'^2 + \frac{G_r}{R_e^2}(\theta - N_r\phi - R_b\Phi) = 0, \tag{10}$$

$$\frac{1}{P_r}\theta'' + \theta'[g + N_b\phi'] + N_t\theta'^2 + E_c\left\{g''^2 + Mg'^2\right\} = 0, \tag{11}$$

$$\phi'' + L_e\phi' g + \frac{N_t}{N_b}\theta'' - L_e\sigma_1(1+\delta\theta)^m e^{\left(\frac{-E}{1+\delta\theta}\right)}\phi = 0, \tag{12}$$

$$\Phi'' + L_b g\Phi' - P_e([\Phi + \Omega_d]\phi'' + \phi'\Phi') = 0. \tag{13}$$

$$g(0) = 0, g'(0) = 1, \theta(0) = \phi(0) = \Phi(0) = 1, \tag{14}$$

$$g'(\infty) = 0, \theta(\infty) = \phi(\infty) = \Phi(\infty) = 0, \tag{15}$$

where

$$\begin{array}{l} \beta_D = \frac{\nu}{a\rho_f k},\ F_r = \frac{C_F x}{\sqrt{k}},\ M = \frac{\sigma {B_0}^2}{a\rho_f},\ \frac{G_r}{R_e^2} = \frac{\overline{g}\beta\left(1-\widetilde{C}_\infty\right)\left(\widetilde{T}-\widetilde{T}_\infty\right)}{a\widetilde{U}_w},\ N_r \\ = \frac{\left(\rho_p-\rho_f\right)\left(\widetilde{C}_w-\widetilde{C}_\infty\right)}{\beta\rho_f\left(\widetilde{T}_w-\widetilde{T}_\infty\right)\left(1-\widetilde{C}_\infty\right)}, P_r = \frac{\nu}{\overline{\alpha}}, R_b = \frac{\gamma\left(\rho_m-\rho_f\right)\left(\widetilde{N}_w-\widetilde{N}_\infty\right)}{\beta\rho_f\left(\widetilde{T}_w-\widetilde{T}_\infty\right)\left(1-\widetilde{C}_\infty\right)},\ N_t \\ = \frac{\overline{\tau}D_T\left(\widetilde{T}_w-\widetilde{T}_\infty\right)}{\nu\widetilde{T}_\infty},\ N_b = \frac{\overline{\tau}D_B\left(\widetilde{C}_w-\widetilde{C}_\infty\right)}{\nu}, E_c = \frac{\widetilde{U}_w{}^2}{c_p\left(\widetilde{T}_w-\widetilde{T}_\infty\right)},\ L_e \\ = \frac{\nu}{D_B},\ \sigma_1 = \frac{{k_r}^2}{a},\ \delta = \frac{\left(\widetilde{T}_w-\widetilde{T}_\infty\right)}{\widetilde{T}_\infty},\ E = \frac{E_a}{k_0\widetilde{T}_\infty} L_b = \frac{\nu}{D_M}, \Omega_d \\ = \frac{\widetilde{N}_\infty}{\left(\widetilde{N}_w-\widetilde{N}_\infty\right)},\ P_e = \frac{bW_C}{D_M}. \end{array} \tag{16}$$

The significant parameters are defined in the list of Nomenclatures.

The shear stress, the local heat, the local mass, and the motile microorganisms' fluxes past the subsurface, imperative parameters, the skin-friction coefficient, the local Sherwood number, the local density number of the motile microorganisms, the local Nusselt number and the local Reynolds number, are respectively defined as

$$\begin{array}{c} \tau_w = \mu\left(\frac{\partial\widetilde{u}}{\partial\hat{y}}\right)_{\hat{y}=0}, q_w = -\kappa\left(\frac{\partial\widetilde{T}}{\partial\hat{y}}\right)_{\hat{y}=0}, q_m = -D_B\left(\frac{\partial\widetilde{C}}{\partial\hat{y}}\right)_{\hat{y}=0}, q_n = -D_M\left(\frac{\partial\widetilde{N}}{\partial\hat{y}}\right)_{\hat{y}=0} \\ C_g Re_x^{1/2} = g''(0), \frac{Nu_x}{Re_x^{1/2}} = -\theta'(0), \frac{Sh_x}{Re_x^{1/2}} = -\phi'(0), \frac{Nn_x}{Re_x^{1/2}} = -\Phi'(0), Re_x = \frac{U_0 x}{\nu}. \end{array} \tag{17}$$

3. Numerical Solution

The implementation of the SLLM to the present system of differential equations needs to reduce the order of Equation (10). In view of the transformation $g' = h$, Equations (10)–(13) can be written as

$$h'' + gh' - h^2 - F_r h^2 - Mh - \beta_D h + \frac{G_r}{R_e^2}(\theta - N_r\phi - R_b\Phi) = 0, \tag{18}$$

$$\frac{1}{P_r}\theta'' + \theta'[g + N_b\phi'] + N_t\theta'^2 + E_c\left\{h'^2 + Mh^2\right\} = 0, \tag{19}$$

$$\phi'' + L_e\phi' g + \frac{N_t}{N_b}\theta'' - L_e\sigma_1(1+\delta\theta)^m e^{\left(\frac{-E}{1+\delta\theta}\right)}\phi = 0, \tag{20}$$

$$\Phi'' + L_b g\Phi' - P_e\left\{[\Phi + \Omega_d]\phi'' + \phi'\Phi'\right\} = 0. \tag{21}$$

By using Taylor's series expansion, the non-linear term "h^2" can be linearized as

$${h^2}_{t+1} = {h^2}_t + 2h_t[h_{t+1} - h_t] = 2h_t h_{t+1} - {h^2}_t. \tag{22}$$

Here, the subscript "t" stands for the previous approximated value, whereas the subscript "$t+1$" stands for the current approximated value.

Now, when we placed Equation (22) in Equation (18), then the non-linear system along with the corresponding boundary conditions are first decoupled by employing the Gauss–Seidel relaxation

method, and then, in view of Chebyshev spectral collocation, the resulting system interims of differentiation matrix "$\boldsymbol{D} = \frac{2}{l}D$" become

$$\boldsymbol{D}g_{t+1} = h_t, \tag{23}$$

$$\left\{\boldsymbol{D}^2 + diag[d_{11}]\boldsymbol{D} - diag[d_{12}]\boldsymbol{I} - d_{13}\boldsymbol{I}\right\}H_{t+1} = d_{1,t}, \tag{24}$$

$$\left\{\frac{1}{P_r}\boldsymbol{D}^2 + diag[d_{11}]\boldsymbol{D} + N_b diag[\phi'_t]\boldsymbol{D} + N_t\boldsymbol{D}^2\right\}\theta_{t+1} = d_{2,t}, \tag{25}$$

$$\left\{\boldsymbol{D}^2 + diag[d_{32}]\boldsymbol{D} + \frac{N_t}{N_b}diag[\theta''_{t+1}] - L_e\sigma_1 diag[d_{33}]e^{\left(\frac{-E}{1+\delta\theta}\right)}\boldsymbol{I}\right\}\phi_{t+1} = d_{3,t}, \tag{26}$$

$$\left\{\begin{array}{c}\boldsymbol{D}^2 + diag[d_{42}]\boldsymbol{D} - P_e\Omega_d diag\left[\phi''_{t+1}\right]\boldsymbol{I} - P_e diag\left[\phi''_{t+1}\right]\boldsymbol{I} \\ -diag\left[\phi'_{t+1}\right]\boldsymbol{D}\end{array}\right\}\Phi_{t+1} = d_{4,t}, \tag{27}$$

with their respective boundary conditions

$$g_{t+1}(\eta_N) = 0, h_{t+1}(\eta_N) = 1 = \theta_{t+1}(\eta_N) = \phi_{t+1}(\eta_N) = \Phi_{t+1}(\eta_N), \tag{28}$$

$$h_{t+1}(\eta_0) = 0 = \theta_{t+1}(\eta_0) = \phi_{t+1}(\eta_0) = \Phi_{t+1}(\eta_0). \tag{29}$$

The system can be expressed in a more simplified way as

$$B_1 g_{t+1} = E_1, \tag{30}$$

$$B_2 h_{t+1} = E_2, \tag{31}$$

$$B_3\theta_{t+1} = E_3, \tag{32}$$

$$B_4\phi_{t+1} = E_4, \tag{33}$$

$$B_5\phi_{t+1} = E_5, \tag{34}$$

where

$$B_1 = \boldsymbol{D}, E_1 = h_t, \tag{35}$$

$$B_2 = \boldsymbol{D}^2 + diag[d_{11}]\boldsymbol{D} - diag[d_{12}]\boldsymbol{I} - d_{13}\boldsymbol{I},\ E_2 = d_{1,t}, \tag{36}$$

$$B_3 = \frac{1}{P_r}\boldsymbol{D}^2 + diag[d_{11}]\boldsymbol{D} + N_b diag[\phi'_t]\boldsymbol{D} + N_t\boldsymbol{D}^2, E_3 = d_{2,t}, \tag{37}$$

$$B_4 = \boldsymbol{D}^2 + diag[d_{32}]\boldsymbol{D} + \frac{N_t}{N_b}diag[\theta''_{t+1}] - L_e\sigma_1 diag[d_{33}]e^{\left(\frac{-E}{1+\delta\theta}\right)}\boldsymbol{I}, E_4 = d_{3,t}, \tag{38}$$

$$\begin{array}{c}B_5 = \boldsymbol{D}^2 + diag[d_{42}]\boldsymbol{D} - P_e\Omega_d diag\left[\phi''_{t+1}\right]\boldsymbol{I} - P_e diag\left[\phi''_{t+1}\right]\boldsymbol{I} \\ -diag\left[\phi'_{t+1}\right]\boldsymbol{D}, E_5 = d_{4,t},\end{array} \tag{39}$$

$$diag[d_{11}] = \begin{bmatrix} d_{11}(\eta_0) & \cdots & \\ \vdots & \ddots & \vdots \\ & \cdots & d_{11}(\eta_N)\end{bmatrix}, diag[d_{12}] = \begin{bmatrix} d_{12}(\eta_0) & \cdots & \\ \vdots & \ddots & \vdots \\ & \cdots & d_{12}(\eta_N)\end{bmatrix},$$

$$diag[d_{1,t}] = \begin{bmatrix} d_{1,t}(\eta_0) \\ \vdots \\ d_{1,t}(\eta_N)\end{bmatrix}, diag[d_{2,t}] = \begin{bmatrix} d_{2,t}(\eta_0) \\ \vdots \\ d_{2,t}(\eta_N)\end{bmatrix}, \tag{40}$$

$$diag[d_{32}] = \begin{bmatrix} d_{32}(\eta_0) & \cdots & \\ \vdots & \ddots & \vdots \\ & \cdots & d_{32}(\eta_N) \end{bmatrix}, diag[d_{33}] = \begin{bmatrix} d_{33}(\eta_0) & \cdots & \\ \vdots & \ddots & \vdots \\ & \cdots & d_{33}(\eta_N) \end{bmatrix},$$

$$diag[d_{42}] = \begin{bmatrix} d_{42}(\eta_0) & \cdots & \\ \vdots & \ddots & \vdots \\ & \cdots & d_{42}(\eta_N) \end{bmatrix}, d_{3,t} = d_{4,t} = 0 = \begin{bmatrix} 0 \\ \vdots \\ 0 \end{bmatrix}. \tag{41}$$

$$g_{t+1} = [g(\eta_0), g(\eta_1), ..., g(\eta_N)]^T, h_{t+1} = [h(\eta_0), h(\eta_1), ..., h(\eta_N)]^T, \tag{42}$$

$$\theta_{t+1} = [\theta(\eta_0), \theta(\eta_1), ..., \theta(\eta_N)]^T, \phi_{t+1} = [\phi(\eta_0), \phi(\eta_1), ..., \phi(\eta_N)]^T, \tag{43}$$

$\Phi_{t+1} = [\Phi(\eta_0), \Phi(\eta_1), ..., \Phi(\eta_N)]^T$ are vectors of sizes $(N+1) \times 1$, while $\mathbf{0}$ is a vector of order $(N+1) \times 1$ and $\boldsymbol{I}$ is an identity matrix of order $(N+1) \times (N+1)$.

The implementation of boundary conditions on the system (23)–(27), yields the following

$$B_1 = \begin{bmatrix} B_1 \\ \hline 0 \quad \dots \quad 1 \end{bmatrix}, g_{t+1} = \begin{bmatrix} g_{t+1}(\eta_0) \\ g_{t+1}(\eta_1) \\ \vdots \\ \hline g_{t+1}(\eta_N) \end{bmatrix},$$

$$E_1 = \begin{bmatrix} E_1 \\ \\ \overline{0} \end{bmatrix}, B_2 = \begin{bmatrix} 1 \quad \dots \quad 0 \\ \hline B_2 \\ \\ \hline 0 \quad \dots \quad 1 \end{bmatrix}, h_{t+1} = \begin{bmatrix} h_{t+1}(\eta_0) \\ \hline h_{t+1}(\eta_1) \\ \vdots \\ \hline h_{t+1}(\eta_N) \end{bmatrix}, \tag{44}$$

$$E_2 = \begin{bmatrix} \underline{0} \\ E_2 \\ \\ \overline{1} \end{bmatrix}, B_3 = \begin{bmatrix} 1 \quad \dots \quad 0 \\ \hline B_3 \\ \\ \hline 0 \quad \dots \quad 1 \end{bmatrix}, \theta_{t+1} = \begin{bmatrix} \theta_{t+1}(\eta_0) \\ \hline \theta_{t+1}(\eta_1) \\ \vdots \\ \hline \theta_{t+1}(\eta_N) \end{bmatrix}, E_3 = \begin{bmatrix} \underline{0} \\ E_3 \\ \\ \overline{1} \end{bmatrix},$$

$$\begin{bmatrix} 1 \quad \dots \quad 0 \\ \hline B_4 \\ \\ \hline 0 \quad \dots \quad 1 \end{bmatrix}, \phi_{t+1} = \begin{bmatrix} \phi_{t+1}(\eta_0) \\ \hline \phi_{t+1}(\eta_1) \\ \vdots \\ \hline \phi_{t+1}(\eta_N) \end{bmatrix}, E_4 = \begin{bmatrix} \underline{0} \\ E_4 \\ \\ \overline{1} \end{bmatrix}, \begin{bmatrix} 1 \quad \dots \quad 0 \\ \hline B_5 \\ \\ \hline 0 \quad \dots \quad 1 \end{bmatrix}, \Phi_{t+1} = \begin{bmatrix} \Phi_{t+1}(\eta_0) \\ \hline \Phi_{t+1}(\eta_1) \\ \vdots \\ \hline \Phi_{t+1}(\eta_N) \end{bmatrix}, \tag{45}$$

$$E_5 = \begin{bmatrix} \underline{0} \\ E_5 \\ \\ \overline{1} \end{bmatrix}.$$

The applicable initial guesses approximation are selected as

$$g_0(\eta) = (1 - e^{-\eta}), h_0(\eta) = e^{-\eta}, \theta_0(\eta) = \phi_0(\eta) = \Phi_0(\eta) = e^{-\eta}. \tag{46}$$

These initial approximation assumptions satisfy the boundary conditions (28) and (29), which subsequently accomplish the approximations of $g_t, h_t, \theta_t, \phi_t, \Phi_t$ for each $t = 1, 2, \dots\dots$ by employing the SLLM technique.

4. Convergence of SLLM Technique

A significant effort was executed to obtain the convergent solutions by employing the successive over-relaxation (SOR) method for each result via this iterative scheme. If "Z" is the resolving function, then the SLLM technique at the $(t+1)$ iteration is

$$B_1 Z_{t+1} = E_1, \tag{47}$$

Now, by revising this, the new mode of the SLLM technique is indicated as

$$B_1 Z_{t+1} = (1-\omega) B_1 Z_t + \omega E_1, \tag{48}$$

where "ω" is the convergence improving the parametric quantity whereas "B_1" and "E_1" represent matrices. This revised SLLM technique improves the accuracy and efficiency of numerical results.

5. Discussion

This section is dedicated to the numerical results, their validation, and the discussion. To inspect the presence of all the leading parameters numerically, the computational software MATLAB was used for the numerical simulations. Table 1 shows the computed convergent outcomes of $Nu_x/Re_x^{1/2}$, $Sh_x/Re_x^{1/2}$ and $Nn_x/Re_x^{1/2}$ across the number of collocation points N, N_t, and N_b by fixing other parameters, whereas Table 2 depicts the comparability of $-\theta'(0), -\phi'(0)$ across N_t and N_b with the preceding investigations by fixing the other parameters of the governing equations. Figures 2–15 have been plotted against all the leading parameters for microorganism distribution, nanoparticle concentration, temperature, and velocity distribution, respectively.

Table 1. Numerical convergent values of Nusselt number, Sherwood Number, and the local density number of the motile microorganisms across N, N_t and N_b by fixing $M = 1, \beta_D = F_r = E_c = \sigma_1 = \delta = E = 0, N_r = 0.5, R_b = 0.5, \frac{G_r}{R_e^2} = 0.5, P_r = 10, L_e = 10, L_b = 2, P_e = 0.5, \Omega_d = 1.0$.

N	N_t	N_b	$\frac{Nu_x}{Re_x^{1/2}}$	$\frac{Sh_x}{Re_x^{1/2}}$	$\frac{Nn_x}{Re_x^{1/2}}$
50	0.3	0.1	1.7573	6.6646	8.4301
60	0.3	0.1	1.7584	6.6658	8.4311
70	0.3	0.1	1.7587	6.6662	8.4314
80	0.3	0.1	1.7587	6.6662	8.4314
100	0.3	0.1	1.7587	6.6662	8.4314
50	0.5	0.5	1.1430	7.7175	9.3273
60	0.5	0.5	1.1446	7.7189	9.3290
70	0.5	0.5	1.1452	7.7198	9.3294
80	0.5	0.5	1.1452	7.7198	9.3294
100	0.5	0.5	1.1452	7.7198	9.3294

Table 2. Comparison of the current outcomes for $-\theta'(0)$ and $-\phi'(0)$ with the previous investigations across N_t and N_b by taking $P_r = L_e = 10, M = \beta_D = F_r = \frac{G_r}{R_e^2} = N_r = R_b = 0, E_c = \sigma_1 = \delta = E = 0$.

N_b	N_t	Current Outcomes for $-\theta'(0)$	Khan and Pop [55]	Current Outcomes for $-\phi'(0)$	Khan and Pop [55]
0.1	0.1	0.952523	0.9524	2.129413	2.1294
	0.2	0.693411	0.6932	2.274116	2.2740
	0.3	0.520134	0.5201	2.528622	2.5286
0.3	0.1	0.252177	0.2522	2.410124	2.4100
	0.2	0.181637	0.1816	2.515065	2.5150
	0.3	0.135610	0.1355	2.608924	2.6088

Figure 2 depicts that the velocity distribution decelerates by enhancing the permeability parameter β_D, and also can be seen as a deceleration in momentum by taking increments of M, due to the existing

body-force brought through the magnetic field, well-known as the Lorentz force, causing a decrement in the velocity overshooting and momentum boundary-layer thickness. In Figure 3, it was reported that the velocity distribution decelerates for both parameters by enhancing the numeric value of these parameters, i.e., the Forchheimer parameter F_r and M. In Figure 4, it is recorded that, by taking the increment in N_r, the velocity distribution decreases as a result of an increment in the negate buoyancy generated through the existence of nanoparticles, while the Richardson number G_r/R_e^2, was boosted by enhancing the values of the Richardson number. Figure 5 portrays that, through an increment in R_b, the velocity distribution decreases because the power of convection due to the bio-convection worked against the convection of buoyancy force, whereas the Richardson number G_r/R_e^2, was boosted by enlarging the values of the Richardson number.

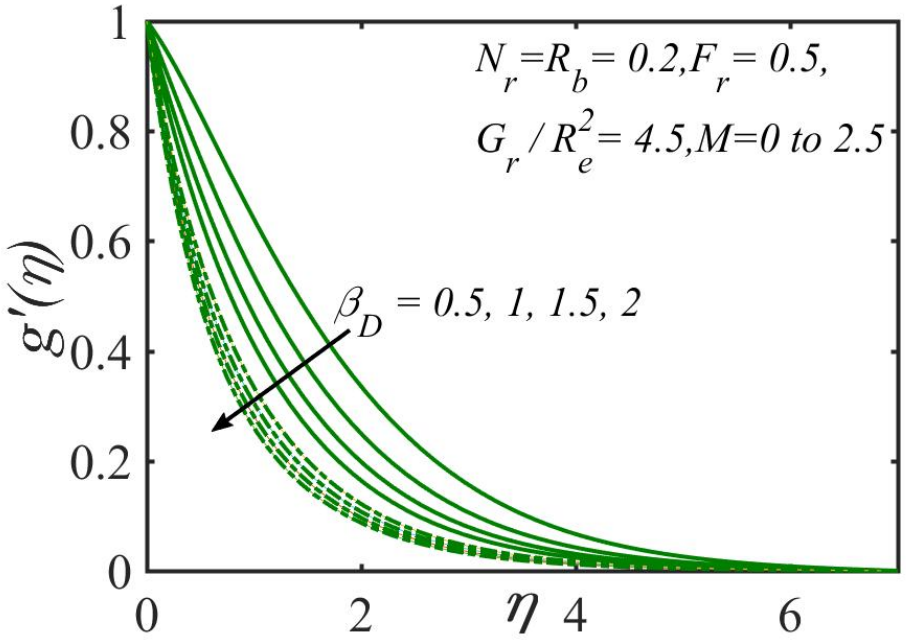

Figure 2. Variation in β_D and M on velocity distribution. Solid line: $M = 0$, Dotted line: $M = 2.5$.

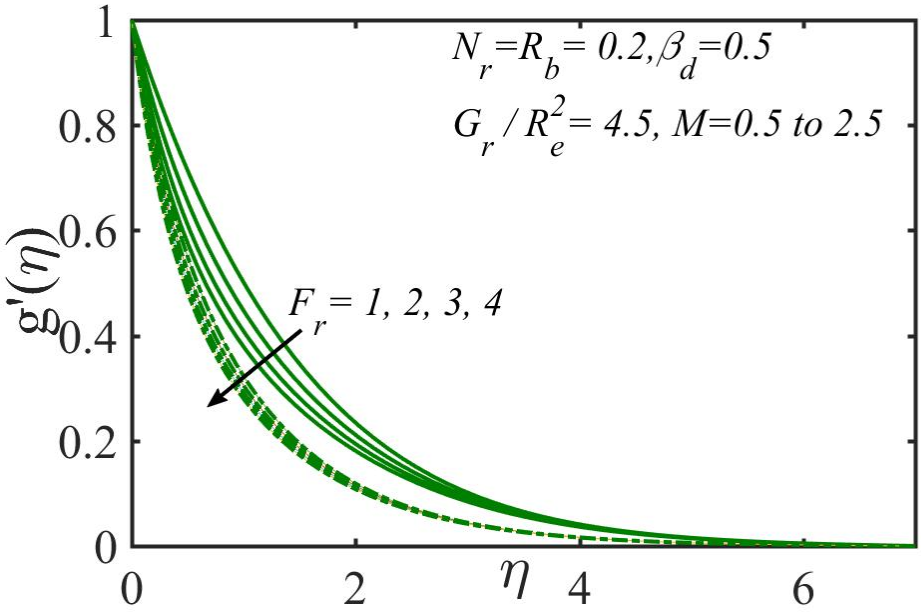

Figure 3. Variation in F_r and M on velocity distribution. Solid line: $M = 0.5$, Dotted line: $M = 2.5$.

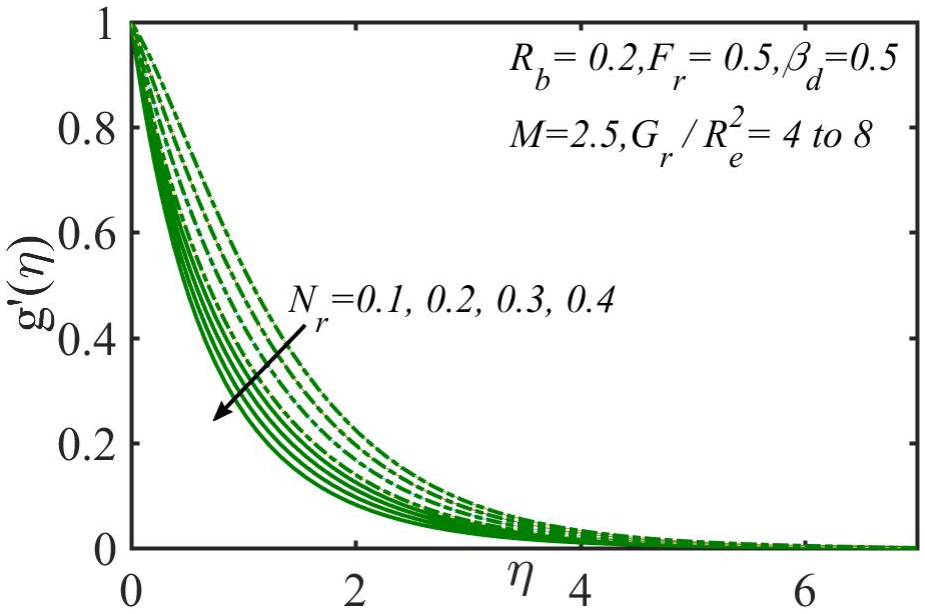

Figure 4. Variation in N_r and $\frac{G_r}{R_e^2}$ on velocity distribution. Solid line: $\frac{G_r}{R_e^2} = 4$, Dotted line: $\frac{G_r}{R_e^2} = 8$.

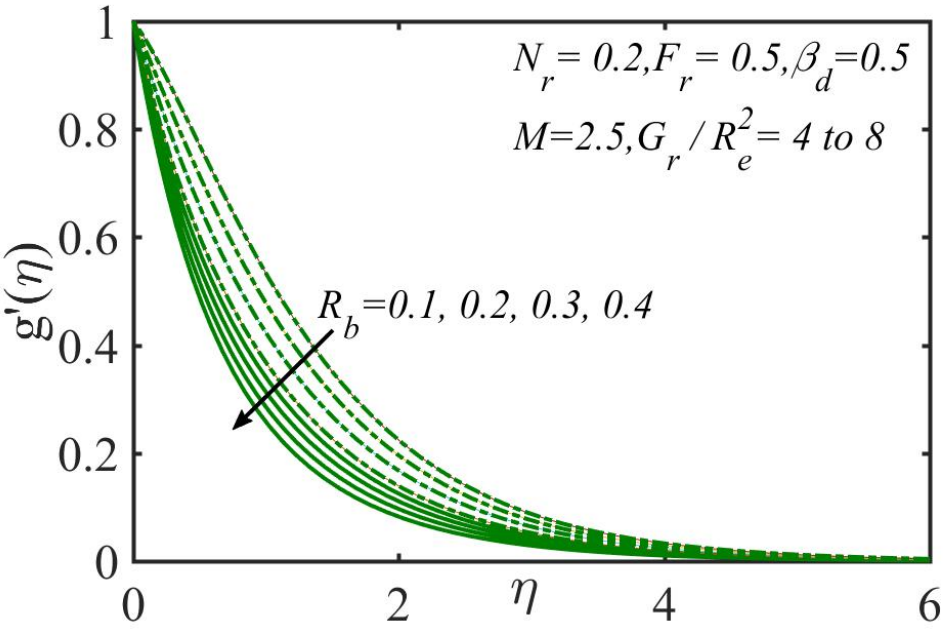

Figure 5. Variation in R_b and $\frac{G_r}{R_e^2}$ on velocity distribution. Solid line: $\frac{G_r}{R_e^2} = 4$ Dotted line: $\frac{G_r}{R_e^2} = 8$.

The impact of the buoyancy proportion parameter N_r, Prandtl number P_r, Hartmann number M, the Brownian-motion parameter N_b, the thermophoresis parameter N_t, local Eckert number E_c, for various numeric values are shown in Figures 6–9. From Figure 6, can be seen that by taking the increment in N_r, the temperature distribution decreases as a result of an increment in the negate buoyancy generated through the existence of nanoparticles, while the Richardson number G_r/R_e^2, it is boosted by enhancing the values of the Richardson number. Figure 7 shows that, by taking an increment in Prandtl number P_r, the temperature distribution slows, although enhancing the thermophoresis parameter N_t accelerates the temperature distribution. Figure 8 shows the effect of thermophoresis parameter N_t and the Brownian-motion parameter N_b of the temperature distribution, and also noticed that the temperature distribution boosts both parameters by enhancing the numeric value of these parameters. The influence of Eckert number E_c and the Brownian-motion parameter N_b of temperature

distribution is shown in Figure 9, and the temperature distribution is boosted for both parameters by enhancing the numeric value of these parameters. Further heating is due to the interaction of the fluid and nanoparticles because of the Brownian-motion, thermophoresis, and viscous dissipation impact. Therefore, the thickness of the thermal boundary layer becomes higher across the larger numeric of N_t, N_b and E_c and temperature overshoots into the neighborhood of the stretched permeable sheet. The impact of the bio-convection Lewis number L_e, the Brownian-motion parameter N_b, the thermophoresis parameter N_t, the chemical reaction constant σ_1, relative temperature parameter δ, the parameter for activation energy E, the bio-convection L_b, Peclet number P_e and the microorganisms' concentration difference parameter Ω_d for concentration distribution and the density of motile microorganisms are shown, respectively, through Figures 10–15. Figure 10 shows the effect of bio-convection Lewis number L_e and the thermophoresis parameter N_t of the concentration distribution and also shows that the concentration distribution decelerates by enhancing the numeric value of Lewis number L_e, because the convection of nanoparticles enhances if we add larger values to Lewis number L_e and are incremented through increases in thermophoresis parameter N_t. Therefore, we suggested that the nanoparticle's boundary layer thickens with N_t. From Figure 11, it observed that, by enlarging the Brownian-motion parameter N_b and the bio-convection Lewis number L_e, the concentration profile slows for both parameters. Figure 12 portrays the influence of the chemical reaction constant σ_1 and the parameter for activation energy E, and shows that ϕ is decelerated with enlarging values of σ_1, while it is incremented with larger values of E. Figure 13 depicts the impact of the relative temperature parameter δ and the parameter for activation energy E, and shows that ϕ earns the largest values for $\delta = -0.5, -0.1, -1.5, -2.0$ and enhances with increments in E. The graphical behavior of various values of the bio-convection L_b and Peclet number P_e in Figure 14 show that a decrement in the density of motile microorganisms quickly occurs by enhancing the bio-convection L_b and Peclet number P_e. That is, the density of motile microorganisms decreases strongly, and by enhancing the bio-convection Lewis number L_b and Peclet number P_e the decrement in microorganisms' diffusion can be calculated, hence the density and boundary layer thickness downturn for motile microorganisms with rising values of L_b and P_e. The power of the Peclet number P_e and the microorganism concentrations' varying parametric quantity Ω_d are shown in Figure 15, and the density of motile microorganisms is decreased by enhancing both the parameters, i.e., the Peclet number P_e and the microorganism concentrations' varying parametric quantity Ω_d.

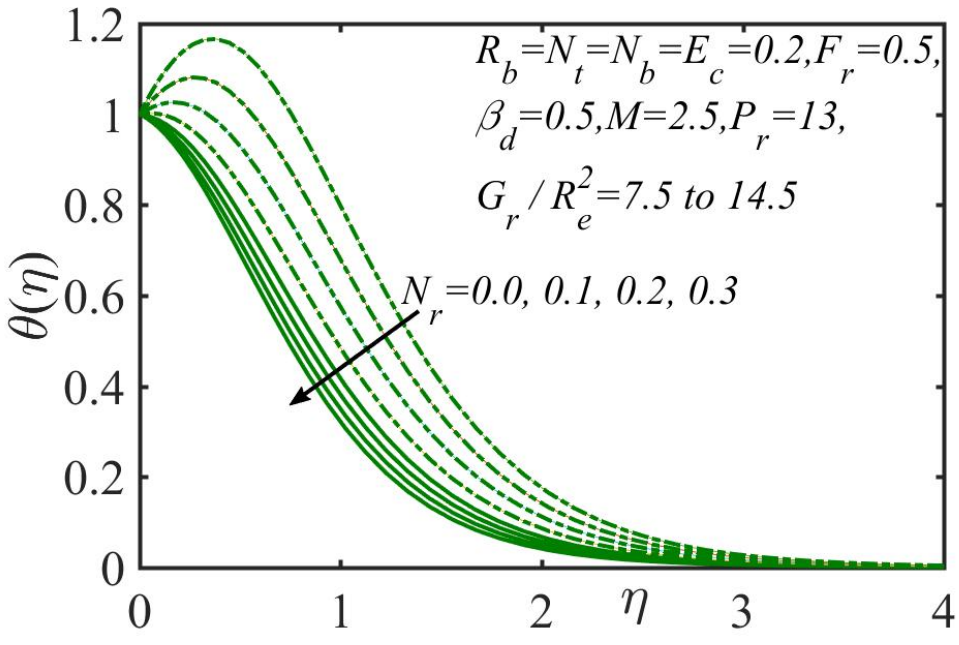

Figure 6. Effect of N_r and $\frac{G_r}{R_e^2}$ on temperature distribution. Solid line: $\frac{G_r}{R_e^2} = 7.5$ Dotted line: $\frac{G_r}{R_e^2} = 14.5$.

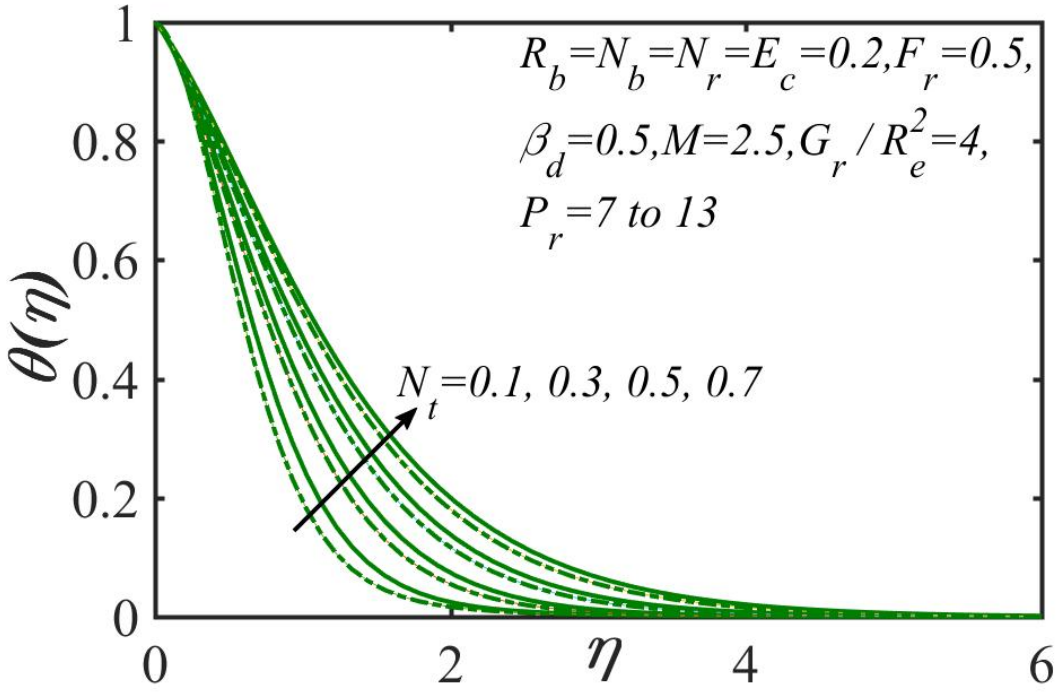

Figure 7. Influence of the thermophoresis parametric quantity N_t and Prandtl number "P_r" on temperature distribution. Solid line: $P_r = 7$, Dotted line: $P_r = 13$.

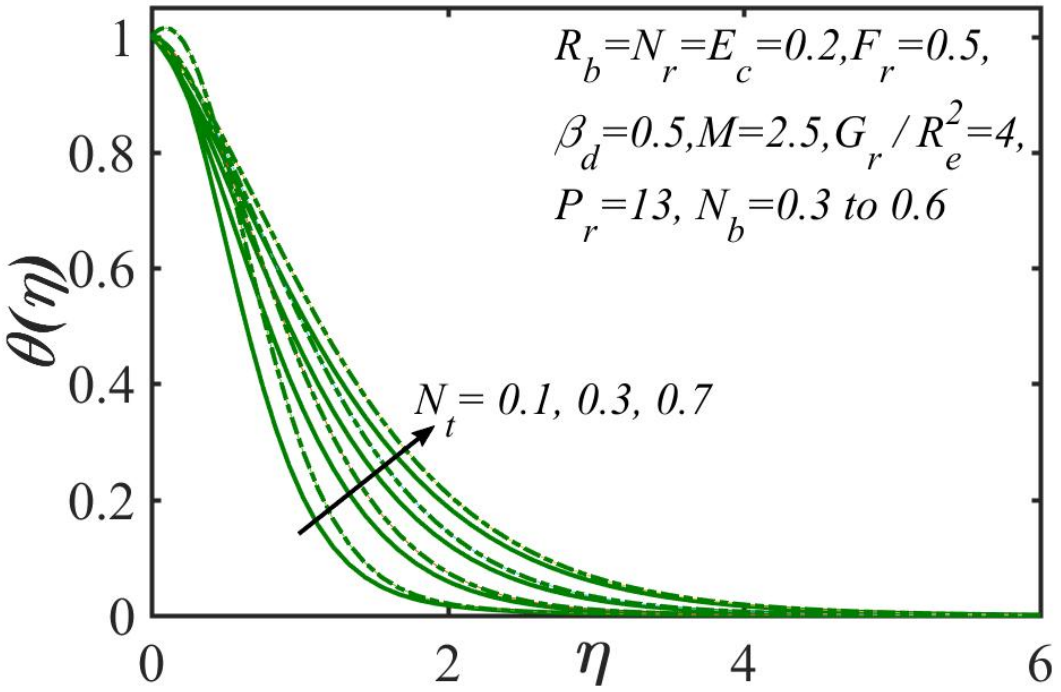

Figure 8. Influence of the thermophoresis parametric quantity N_t and the Brownian-motion parameter "N_b" on temperature distribution. Solid line: $N_b = 0.3$, Dotted line: $N_b = 0.6$.

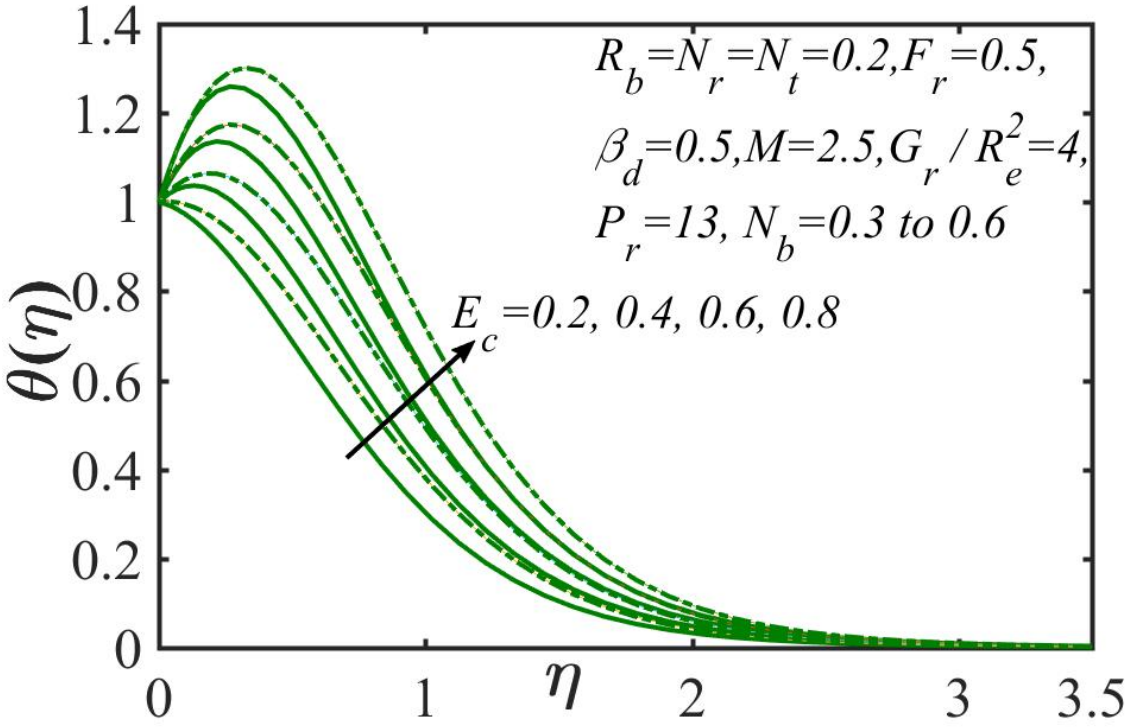

Figure 9. Effect of the Eckert number E_c and the Brownian motion parameter "N_b" on temperature distribution. Solid line: $N_b = 0.3$, Dotted line: $N_b = 0.6$.

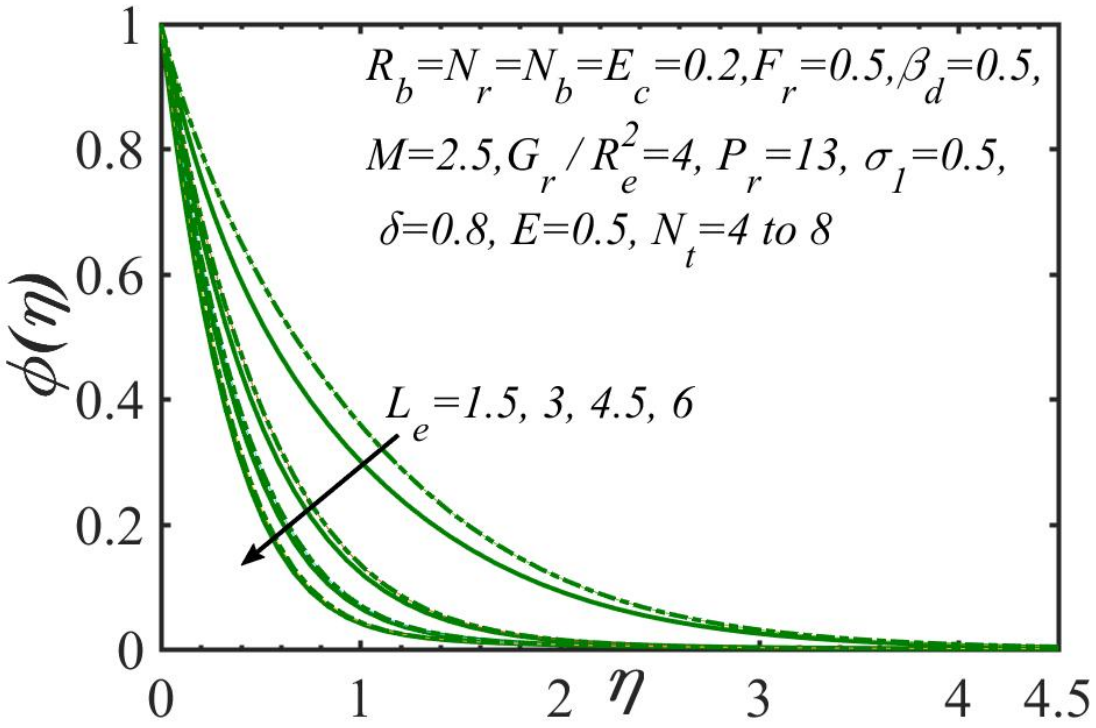

Figure 10. Influence of the bio-convection Lewis number L_e and the thermophoresis parameter "N_t" on concentration distribution. Solid line: $N_t = 4$, Dotted line: $N_t = 8$.

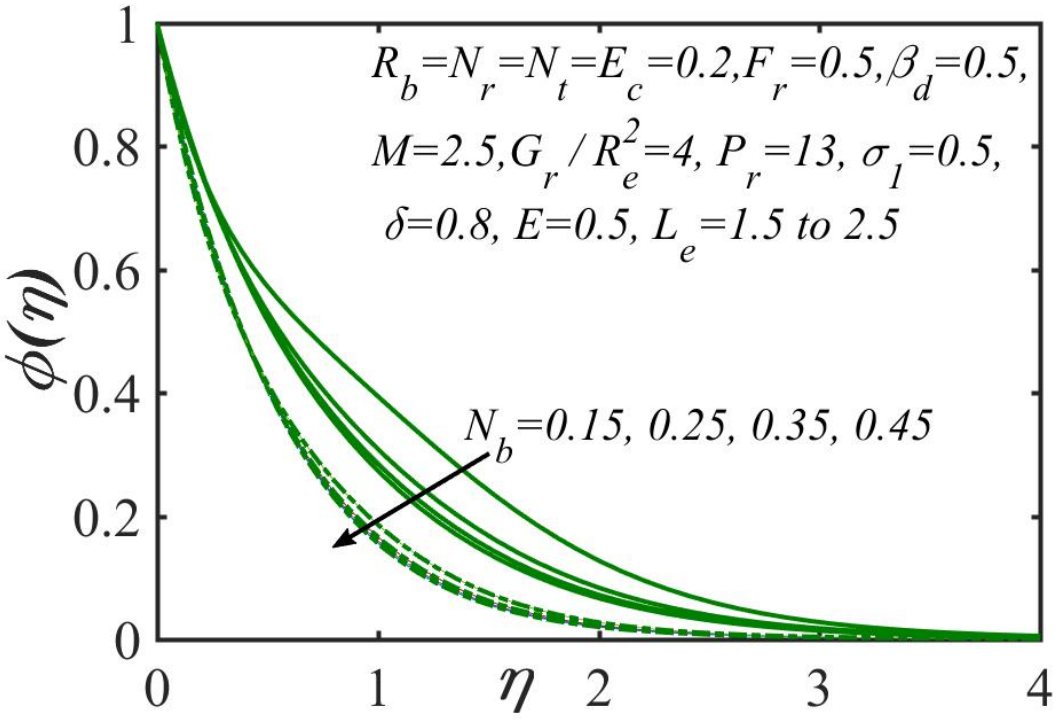

Figure 11. Influence of the Brownian-motion parameter N_b and the bio-convection Lewis number "L_e" on concentration distribution. Solid line: $L_e = 1.5$, Dotted line: $L_e = 2.5$.

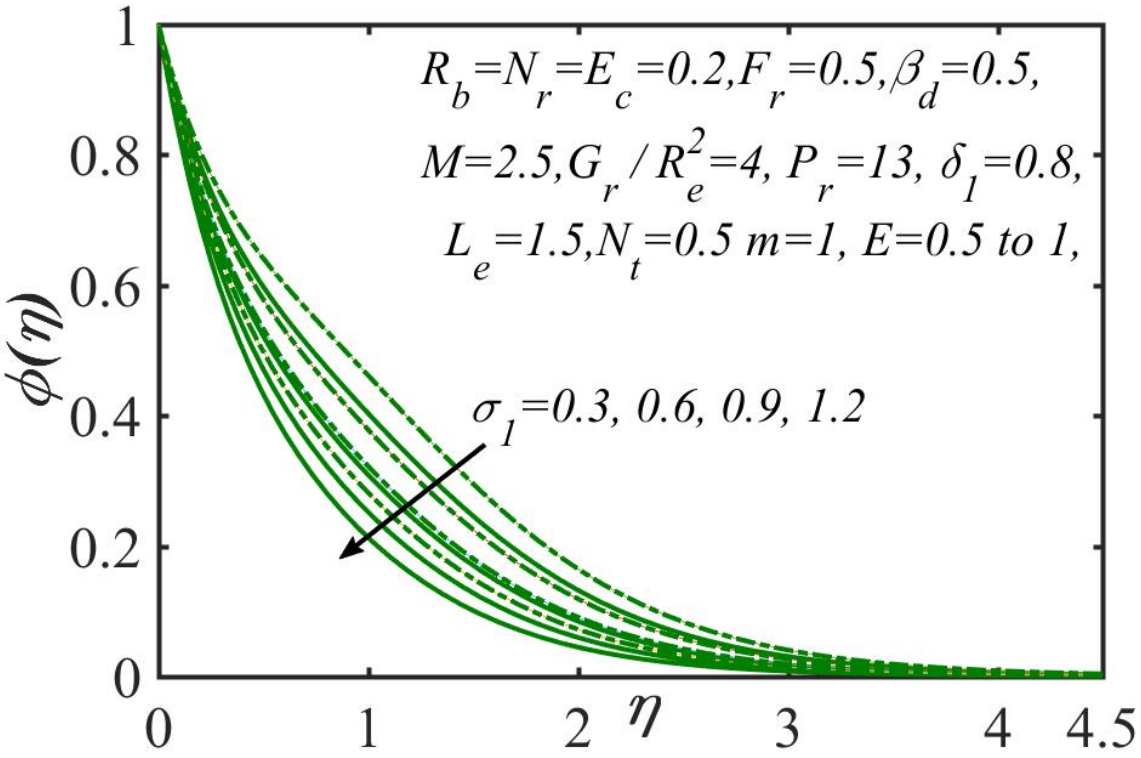

Figure 12. Variation in σ_1 and E on concentration distribution. Solid line: $E = 0.5$, Dotted line: $E = 1.0$.

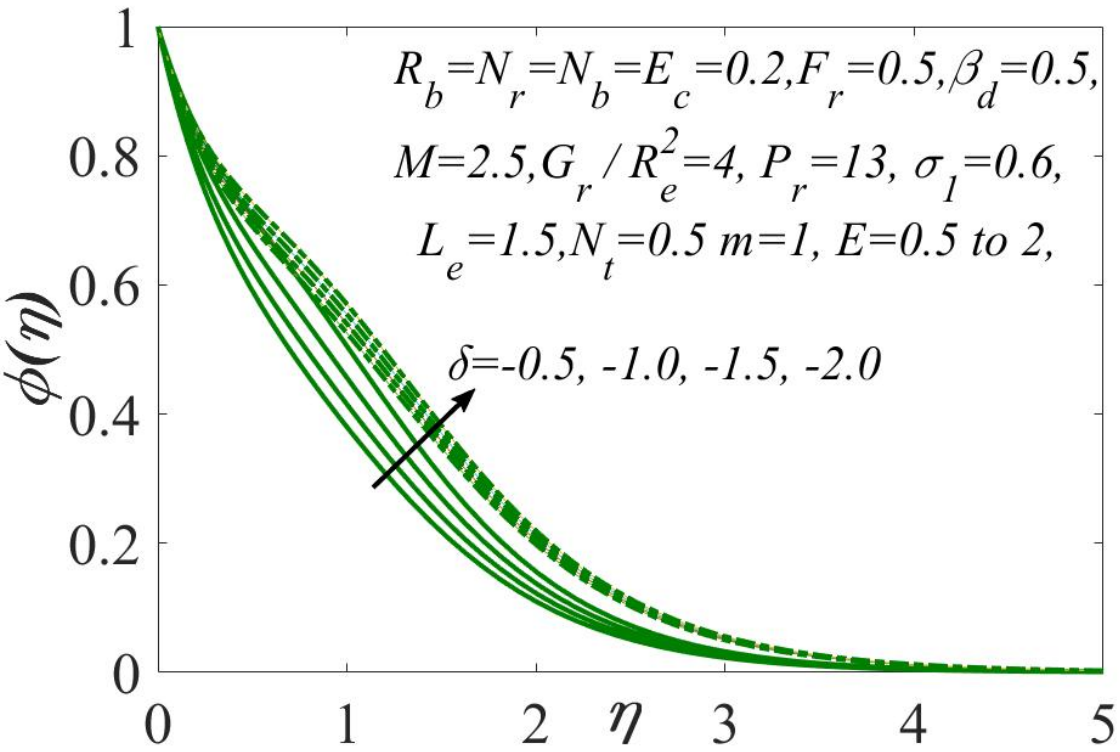

Figure 13. Variation in δ and E on concentration distribution. Solid line: $E = 0.5$, Dotted line: $E = 2.0$.

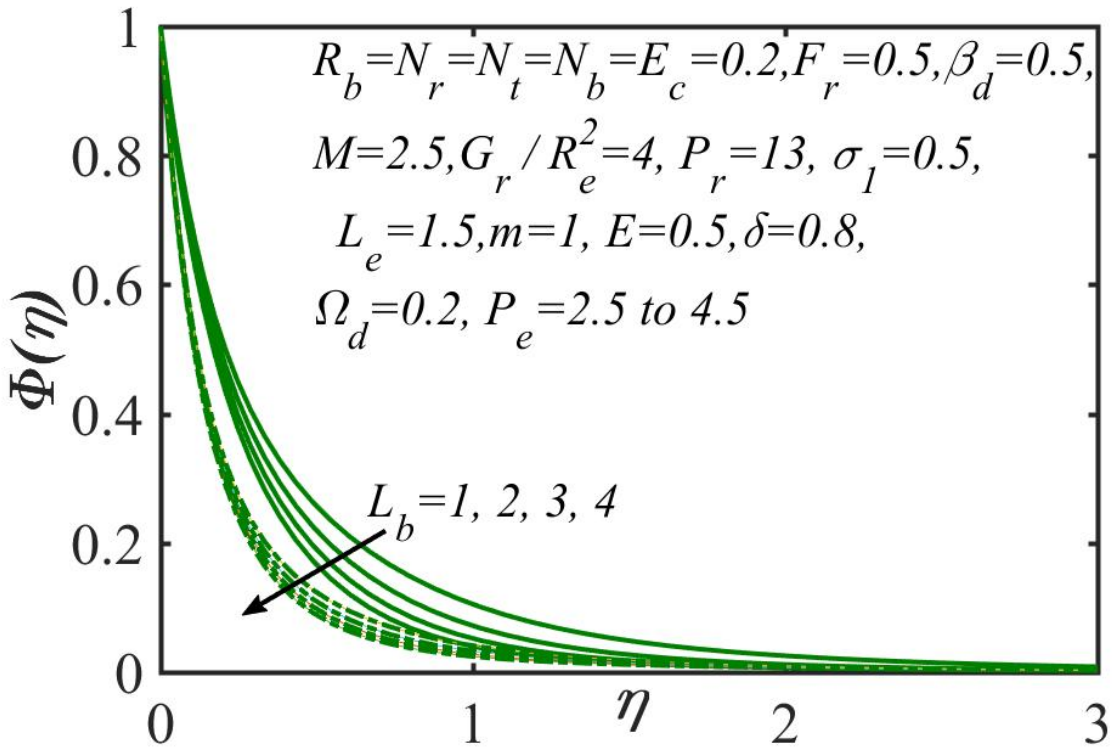

Figure 14. Effect of the bio-convection Lewis number L_b and Peclet number P_e on the density of motile microorganisms. Solid line: $P_e = 2.5$, Dotted line: $P_e = 4.5$.

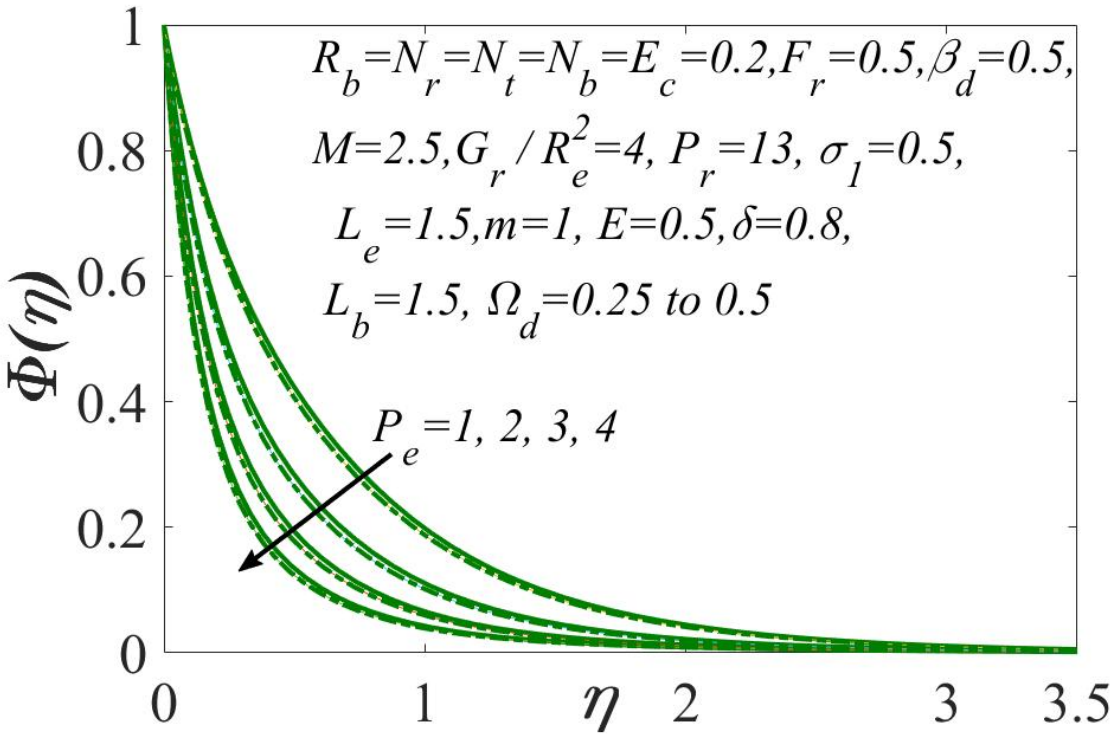

Figure 15. Effect of the Peclet number P_e and the microorganisms concentration variance parametric quantity Ω_d on the density of motile microorganisms. Solid line: $\Omega_d = 0.25$, Dotted line: $\Omega_d = 0.5$.

6. Conclusions

The notable results of the current investigation are:

i. The successive local linearization method is found to be very stable and flexible for resolving nonlinear magnetic materials' processing transport phenomena problems;
ii. The numerical efficiency of SLLM is powerful, because it develops in a series of equations which are solved by reutilizing the data from the solution of one equation in the next equation;
iii. Due to its accuracy, efficiency, and smoothness, it is visualized that the proposed SLLM technique could be employed as a feasible technique for solving certain classes of boundary layer fluid flow problems;
iv. Furthermore, in the present investigation, we have ignored the behavior of non-Newtonian nanofluid models and double-diffusive convection flows, which can be considered in the upcoming articles.

Author Contributions: Conceptualization, R.E.; Investigation, M.M.B.; Methodology, A.S.; Validation, T.A.; Writing—review & editing, S.Z.A. All authors have read and agreed to the published version of the manuscript.

Funding: This research was funded by King Fahd University of Petroleum & Minerals, Dhahran, Saudi Arabia (ORCP2500).

Acknowledgments: R. Ellahi gratefully thanks to King Fahd University of Petroleum & Minerals, Dhahran, Saudi Arabia to honor him with the Chair Professor at KFUPM.

Conflicts of Interest: The authors declare no conflict of interest.

Nomenclatures

$\widetilde{u}, \widetilde{v}$	Components of velocity
$\overline{k}$	Thermal conductivity
a, b	Constants
g	Dimensionless stream function
$\overline{g}$	Gravity
$C_{g\hat{x}}$	Skin friction coefficient
$Sh_{\hat{x}}$	Sherwood number
$Nn_{\hat{x}}$	Local-density number of motile microorganisms
$Nu_{\hat{x}}$	Nusselt number
$\left[c_p\right]_f$	Heat capacity
B_0	Magnetic field
C_F	Forchheimer coefficient
q_w	Local heat flux past the surface
$\widetilde{T}_w$	Temperature of the wall
k_0	Boltzmann constant
$\widetilde{T}_\infty$	Ambient temperature
k	Porosity parameter
$\widetilde{p}$	Pressure
$\left(c_p\right)_s$	Heat capacity of solid fraction
$\widetilde{U}_w$	Stretching sheet velocity
$\hat{x}, \hat{y}$	Cartesian coordinates along the surface
$\widetilde{C}$	The concentration for nanoparticle
P_r	Prandtl number
$\widetilde{N}$	Density for motile microorganism
$\boldsymbol{D}_B$	Brownian-diffusion coefficient
$\mathrm{D_M}$	Diffusivity of microorganisms
$\left[c_p\right]_p$	Nanoparticles heat capacity
Re_x	Local Reynolds number
$\boldsymbol{D}_T$	Thermophoresis diffusion coefficient
W_C	Heat capacitance of the nanoparticle
M	Hartmann number
G_r/R_e^2	The local Richardson number
N_r	Buoyancy proportion parameter
N_b	Brownian motion parameter
m	Dimensionless exponent
R_b	Bioconvection Rayleigh number
N_t	Thermophoresis parameter
E_c	Eckert number
E_a	Activation energy
L_b	Bioconvection Lewis number
k_r	Chemical reaction rate
L_e	Lewis number
P_e	Bio-convection Peclet number
q_m	Local mass flux past the surface

Greek Symbols

κ_{nf}	Thermal conductivity of nanofluid
Φ	Motile microorganism profile
ϕ	Concentration profile
μ_{nf}	Dynamic viscosity
θ	Temperature profile
ν_{nf}	Kinematic viscosity of nanofluid
κ_{nf}	Thermal conductivity of nanofluid
ρ_f	Density of the fluid
σ	Electrical conductivity
τ_w	Shear stress
ρ_m, ρ_p	Densities of microorganisms and nanoparticles
Ω_d	Microorganisms concentration variance parameter
γ	Average volume for a microorganism
$\overline{\alpha}$	Thermal diffusivity
β_D	Permeability parameter

References

1. Buongiorno, J. Convective transport in nanofluids. *ASME J. Heat Transf.* **2006**, *128*, 240–250. [CrossRef]
2. Tiwari, R.K.; Das, M.K. Heat transfer augmentation in a two-sided lid driven differentially heated cavity utilizing nanofluids. *Int. J. Heat Mass Transf.* **2007**, *50*, 2002–2018. [CrossRef]
3. Kuznetsov, A.V.; Nield, D.A. Natural convective boundary-layer flow of a nanofluid past a vertical plate. *Int. J. Therm. Sci.* **2010**, *49*, 243–247. [CrossRef]
4. Awais, M.; Hayat, T.; Irum, S.; Alsaedi, A. Heat Generation/Absorption Effects in a Boundary Layer Stretched Flow of Maxwell Nanofluid: Analytic and Numeric Solutions. *PLoS ONE* **2015**, *10*, e0129814. [CrossRef] [PubMed]
5. Ghalambaz, M.; Sheremet, M.A.; Pop, I. Free Convection in a Parallelogrammic Porous Cavity Filled with a Nanofluid Using Tiwari and Das' Nanofluid Model. *PLoS ONE* **2015**, *10*, e0126486. [CrossRef] [PubMed]
6. Choi, S.; Zhang, Z.; Yu, W.; Lockwood, F.; Grulke, E. Anomalous thermal conductivity enhancement in nanotube suspensions. *Appl. Phys. Lett.* **2001**, *79*, 2252–2254. [CrossRef]
7. Ellahi, R.; Hussain, F.; Abbas, S.A.; Sarafraz, M.M.; Goodarzi, M.; Shadloo, M.S. Study of two-phase Newtonian nanofluid flow hybrid with hafnium particles under the effects of slip. *Invention* **2020**, *5*, 6. [CrossRef]
8. Majeed, A.; Zeeshan, A.; Alamri, S.Z.; Ellahi, R. Heat transfer analysis in ferromagnetic viscoelastic fluid flow over a stretching sheet with suction. *Neural Comput. Appl.* **2018**, *30*, 1947–1955. [CrossRef]
9. Noghrehabadadi, A.; Pourrajab, R.; Ghalambaz, M. Flow and heat transfer of nanofluids over stretching sheet taking into account partial slip and thermal convective boundary conditions. *Heat Mass Transf.* **2013**, *49*, 1357–1366. [CrossRef]
10. Nilson, R.H.; Griffiths, S.K. Influence of atomistic physics on electro-osmotic flow: An analysis based on density functional theory. *J. Chem. Phys.* **2006**, *125*, 164510. [CrossRef]
11. Lee, J.W.; Nilson, R.H.; Templeton, J.A.; Griffiths, S.K.; Kung, A.; Wong, B.M. Comparison of molecular dynamics with classical density functional and poisson–boltzmann theories of the electric double layer in nanochannels. *J. Chem. Theory Comput.* **2012**, *8*, 2012–2022. [CrossRef]
12. Wakif, A.; Animasaun, I.L.; Satya Narayana, P.V.; Sarojamma, G. Meta-analysis on thermo-migration of tiny/nano-sized particles in the motion of various fluids. *Chin. J. Phys.* **2019**. [CrossRef]
13. Shahsavar, A.; Godini, A.; Sardari, P.T.; Toghraie, D.; Salehipour, H. Impact of variable fluid properties on forced convection of Fe_3O_4/CNT/water hybrid nanofluid in a double-pipe mini-channel heat exchanger. *J. Therm. Anal. Calorim.* **2019**, *37*, 1031–1043. [CrossRef]
14. Barnoon, P.; Toghraie, D.; Eslami, F.; Mehmandoust, B. Entropy generation analysis of different nanofluid flows in the space between two concentric horizontal pipes in the presence of magnetic field: Single-phase and two-phase approaches. *Comput. Math. Appl.* **2019**, *77*, 662–692. [CrossRef]

15. Maleki, H.; Safaei, M.R.; Togun, H.; Dahari, M. Heat transfer and fluid flow of pseudo-plastic nanofluid over a moving permeable plate with viscous dissipation and heat absorption/generation. *J. Therm. Anal. Calorim.* **2019**, *135*, 1643–1654. [CrossRef]
16. Maleki, H.; Safaei, M.R.; Alrashed, A.A.; Kasaeian, A. Flow and heat transfer in non-Newtonian nanofluids over porous surfaces. *J. Therm. Anal. Calorim.* **2019**, *135*, 1655–1666. [CrossRef]
17. Hiemenz, K. The boundary layer on a circular cylinder in uniform flow (in German). *Dingl. Polytech. J.* **1911**, *326*, 321–328.
18. Chiam, T.C. Stagnation point flow towards a stretching plate. *J. Phys. Soc. Jpn.* **1994**, *63*, 2443–2444. [CrossRef]
19. Asma, M.; Othman, W.A.M.; Muhammad, T.; Mallawi, F.; Wong, B.R. Numerical study for magnetohydrodynamic flow of nanofluid due to a rotating disk with binary chemical reaction and Arrhenius activation energy. *Symmetry* **2019**, *11*, 1282. [CrossRef]
20. Makinde, O.D.; Animasaun, I. Bioconvection in MHD nanofluid flow with nonlinear thermal radiation and quartic autocatalysis chemical reaction past an upper surface of a paraboloid of revolution. *Int. J. Therm. Sci.* **2016**, *109*, 159–171. [CrossRef]
21. Ellahi, R.; Sait, S.M.; Shehzad, N.; Ayaz, Z. A hybrid investigation on numerical and analytical solutions of electro-magnetohydrodynamics flow of nanofluid through porous media with entropy generation. *Int. J. Numer. Methods Heat Fluid Flow* **2020**, *30*, 834–854. [CrossRef]
22. Sarafraz, M.M.; Pourmehran, O.; Yang, B.; Arjomandi, M.; Ellahi, R. Pool boiling heat transfer characteristics of iron oxide nano-suspension under constant magnetic field. *Int. J. Therm. Sci.* **2020**, *147*, 106131. [CrossRef]
23. Ellahi, R. Special issue on symmetry and fluid mechanics. *Symmetry* **2020**, *12*, 281. [CrossRef]
24. Majeed, A.; Zeeshan, A.; Bhatti, M.M.; Ellahi, R. Heat transfer in magnetite (Fe_3O_4) nanoparticles suspended with conventional fluids: Refrigerant-134a (C2H2F4), kerosene (C10H22) and water (H_2O) under the impact of dipole. *Heat Transf. Res.* **2020**, *51*, 217–232. [CrossRef]
25. Wakif, A.; Boulahia, Z.; Ali, F.; Eid, M.R.; Sehaqui, R. Numerical analysis of the unsteady natural convection MHD Couette nanofluid flow in the presence of thermal radiation using single and two-phase nanofluid models for Cu-water nanofluids. *Int. J. Appl. Comput. Math.* **2018**, *4*, 81. [CrossRef]
26. Wakif, A.; Qasim, M.; Afridi, M.I.; Saleem, S.; Al-Qarni, M.M. Numerical examination of the entropic energy harvesting in a magnetohydrodynamic dissipative flow of stokes' second problem: Utilization of the gear-generalized differential quadrature method. *J. Non-Equilib. Thermodyn.* **2019**, *44*, 385–403. [CrossRef]
27. Mousavi, S.M.; Darzi, A.A.R.; Akbari, O.A.; Toghraie, D.; Marzban, A. Numerical study of biomagnetic fluid flow in a duct with a constriction affected by a magnetic field. *J. Magn. Magn. Mater.* **2019**, *473*, 42–50. [CrossRef]
28. Afrand, M.; Sina, N.; Teimouri, H.; Mazaheri, A.; Safaei, M.R.; Esfe, M.H.; Kamali, J.; Toghraie, D. Effect of magnetic field on free convection in inclined cylindrical annulus containing molten potassium. *Int. J. Appl. Mech.* **2015**, *7*, 1550052. [CrossRef]
29. Khodabandeh, E.; Akbari, O.A.; Akbari, S.; Taghizadeh, A.; Pour, M.S.; Ersson, M.; Jönsson, P.G. The effects of oil/MWCNT nanofluids and geometries on the solid oxide fuel cell cooling systems: A CFD study. *J. Therm. Anal. Calorim.* **2020**. [CrossRef]
30. Varzaneh, A.A.; Toghraie, D.; Karimipour, A. Comprehensive simulation of nanofluid flow and heat transfer in straight ribbed microtube using single-phase and two-phase models for choosing the best conditions. *J. Therm. Anal. Calorim.* **2020**, *139*, 701–720. [CrossRef]
31. Jamali, M.; Toghraie, D. Investigation of heat transfer characteristics in the developing and the developed flow of nanofluid inside a tube with different entrances in the transition regime. *J. Therm. Anal. Calorim.* **2019**. [CrossRef]
32. Al-Rashed, A.A.A.A.; Shahsavar, A.; Akbari, M.; Toghraie, D.; Akbari, M.; Afrand, M. Finite volume simulation of mixed convection in an inclined lid-driven cavity filled with nanofluids: Effects of a hot elliptical centric cylinder, cavity angle and volume fraction of nanoparticles. *Phys. A Stat. Mech. Appl.* **2019**, *527*, 121122. [CrossRef]
33. Alrashed, A.A.A.A.; Akbari, O.A.; Toghraie, D.; Zarringhalam, M.; Shabani, G.A.S.; Seifi, A.R.; Goodarzi, M. The numerical modeling of water/FMWCNT nanofluid flow and heat transfer in a backward-facing contracting channel. *Phys. B Condens. Matter* **2018**, *537*, 176–183. [CrossRef]

34. Mostafazadeh, A.; Toghraie, D.; Mashayekhi, R.; Akbari, O.A. Effect of radiation on laminar natural convection of nanofluid in a vertical channel with single- and two-phase approaches. *J. Therm. Anal. Calorim.* **2019**, *138*, 779–794. [CrossRef]
35. Li, Z.X.; Barnoon, P.; Toghraie, D.; Dehkordi, R.B.; Afrand, M. Mixed convection of non-Newtonian nanofluid in an H-shaped cavity with cooler and heater cylinders filled by a porous material: Two phase approach. *Adv. Powder Technol.* **2019**, *30*, 2666–2685. [CrossRef]
36. Khodabandeh, E.; Rozati, S.A.; Joshaghani, M.; Akbari, O.A.; Akbari, S.; Toghraie, D. Thermal performance improvement in water nanofluid/GNP–SDBS in novel design of double-layer microchannel heat sink with sinusoidal cavities and rectangular ribs. *J. Therm. Anal. Calorim.* **2019**, *136*, 1333–1345. [CrossRef]
37. Alamri, S.Z.; Ellahi, R.; Shehzad, N.; Zeeshan, A. Convective radiative plane Poiseuille flow of nanofluid through porous medium with slip: An application of Stefan blowing. *J. Mol. Liq.* **2019**, *273*, 292–304. [CrossRef]
38. Alamri, S.Z.; Khan, A.A.; Azeez, M.; Ellahi, R. Effects of mass transfer on MHD second grade fluid towards stretching cylinder: A novel perspective of Cattaneo–Christov heat flux model. *Phys. Lett. A* **2019**, *383*, 276–281. [CrossRef]
39. Sajid, T.; Sagheer, M.; Hussain, S.; Bilal, M. Darcy-Forchheimer flow of Maxwell nanofluid flowwith nonlinear thermal radiation and activation energy. *AIP Adv.* **2018**, *8*, 035102. [CrossRef]
40. Khan, M.I.; Hayat, T.; Khan, M.I.; Alsaedi, A. Activation energy impact in nonlinear radiative stagnation point flow of Cross nanofluid. *Int. Commun. Heat Mass* **2018**, *91*, 216–224. [CrossRef]
41. Khan, S.U.; Waqas, H.; Shehzad, S.A.; Imran, M. Theoretical analysis for tangent hyperbolic nanoparticles with combined electrical MHD, activation energy and Wu's slip features: A mathematical model. *Phys. Scr.* **2019**, *94*, 125211. [CrossRef]
42. Zeeshan, A.; Shehzad, N.; Ellahi, R. Analysis of activation energy in Couette-Poiseuille flow of nanofluid in the presence of chemical reaction and convective boundary conditions. *Results Phys.* **2018**, *8*, 502–512. [CrossRef]
43. Ellahi, R.; Zeeshan, A.; Hussain, F.; Asadollahi, A. Peristaltic blood flow of couple stress fluid suspended with nanoparticles under the influence of chemical reaction and activation energy. *Symmetry* **2019**, *11*, 276. [CrossRef]
44. Khan, S.U.; Waqas, H.; Bhatti, M.M.; Imran, M. Bioconvection in the Rheology of Magnetized Couple Stress Nanofluid Featuring Activation Energy and Wu's Slip. *J. Non-Equilib. Thermodyn.* **2020**, *45*, 81–95. [CrossRef]
45. Kuznetsov, A.V.; Avramenko, A.A. Effect of small particles on the stability of bioconvection in a suspension of gyrotactic microorganisms in a layer of finite depth. *Int. Commun. Heat Mass* **2004**, *31*, 1–10. [CrossRef]
46. Kuznetsov, A.V.; Geng, P. The interaction of bioconvection caused by gyrotactic micro-organisms and settling of small solid particles. *Int. J. Numer. Method H* **2005**, *15*, 328–347. [CrossRef]
47. Lee, J.J.; Kim, H.J.; Kim, D.K. Experimental study on forced convection heat transfer from plate-fin heat sinks with partial heating. *Processes* **2019**, *7*, 772. [CrossRef]
48. Khan, W.A.; Makinde, O.D. MHD nanofluid bioconvection due to Gyrotactic Microorganisms over a Convectively heat stretching sheet. *Int. J. Therm. Sci.* **2014**, *81*, 118–124. [CrossRef]
49. Raees, A.; Hang, X.U.; Qiang, S.U.N.; Pop, I. Mixed convection in gravity-driven nano-liquid film containing both nanoparticles and gyrotactic microorganisms. *Appl. Math. Mech.* **2015**, *36*, 163–178. [CrossRef]
50. Shahid, A.; Zhou, Z.; Bhatti, M.M.; Tripathi, D. Magnetohydrodynamics Nanofluid Flow Containing Gyrotactic Microorganisms Propagating Over a Stretching Surface by Successive Taylor Series Linearization Method. *Microgravity Sci. Technol.* **2018**, *30*, 445–455. [CrossRef]
51. Waqas, H.; Khan, S.U.; Imran, M.; Bhatti, M.M. Thermally developed Falkner–Skan bioconvection flow of a magnetized nanofluid in the presence of a motile gyrotactic microorganism: Buongiorno's nanofluid model. *Phys. Scr.* **2019**, *94*, 115304. [CrossRef]
52. Trefethen, L.N. *Spectral Methods in MATLAB*; SIAM: Philadelphia, PA, USA, 2000; Volume 10.
53. Bhatti, M.M.; Abbas, M.A.; Rashidi, M.M. A robust numerical method for solving stagnation point flow over a permeable shrinking sheet under the influence of MHD. *Appl. Math. Comp.* **2018**, *316*, 381–389. [CrossRef]

54. Mehryan, S.A.M.; Kashkooli, F.M.; Soltani, M.; Raahemifar, K. Fluid flow and heat transfer analysis of a nanofluid containing motile gyrotactic micro-organisms passing a nonlinear stretching vertical sheet in the presence of a non-uniform magnetic field; numerical approach. *PLoS ONE* **2016**, *11*, e0157598. [CrossRef] [PubMed]
55. Khan, W.A.; Pop, I. Boundary-layer flow of a nanofluid past a stretching sheet. *Int. J. Heat Mass Transf.* **2010**, *53*, 2477–2483. [CrossRef]